# New Technique for Synthesizing Iron Ferrite Magnetic Nanosized Particles

**ARTICLE** *in* LANGMUIR · JULY 1997

Impact Factor: 4.46 · DOI: 10.1021/la960854q



**2 AUTHORS**, INCLUDING:

Nicolas Feltin
Laboratoire National de Métrologie et d'Essais
**52** PUBLICATIONS **590** CITATIONS

# New Technique for Synthesizing Iron Ferrite Magnetic Nanosized Particles

N. Feltin[†,‡] and M. P. Pileni*[,†,‡]

*Laboratoire SRSI, URA CNRS 1662, Universite P et M Curie (Paris VI), BP 52, 4 Place Jussieu, 75231 Paris cedex 05, France, and CEA−CE Saclay, DRECAM-SCM, 91191 Gif sur Yvette,Cedex, France*

*Received September 3, 1996. In Final Form: December 20, 1996*[⊗]

Ferrous dodecyl sulfate, $Fe(DS)_2$, micellar solution was used to make nanosized magnetic particles whose size is controlled by the surfactant concentration and by temperature. The average particle size varies from 3.7 to 11.6 nm, with a standard deviation ranging from 0.22 to 0.34. In contrast to what is obtained in homogeneous solution, iron ferrite particles can be obtained when the synthesis is performed at very low reactant concentrations and room temperature. Furthermore, nanoparticles are obtained when the syntheses are performed using Fe(II) as reactant whereas in homogeneous solution particles in the micrometric range are formed. The particle crystallinity varies with the synthesis temperature, going from fairly low values at 25 °C to fairly high values at 50 °C and above. The particles are characterized by superparamagnetic behavior. The saturation magnetization decreases with particle size, which is explained in terms of non-collinear structure at the interface. Particles with low crystallinity are characterized by magnetic diameters smaller than those determined by transmission electron microscopy. This is attributed to crystalline anisotropy.

## I. Introduction

The creation of perfect nanometer-scale crystallites (quantum crystals) identically replicated in unlimited quantities in a state than can be manipulated and behave as pure macromolecular substances is an ultimate challenge in modern materials research with outstanding fundamental and potential technological consequences.

Due to their small size, the nanoparticles exhibit novel material properties which largely differ from the bulk solid state.[1,2] Many reports on quantum size effects on semiconductors[3,4] or the emergence of metallic properties dependent on the particle size[5,6] have been published in the last few years.

A better understanding of magnetism is crucial not only for basic physics but also because of the great technological importance of ferromagnets in information storage,[7] color imaging,[8] bioprocessing,[9] and ferrofluids.[10] Ferromagnetism occurs even for clusters with less than about 30 atoms. As the size increases up to 700 atoms, the magnetic moments approach the bulk limit.[11]

Fine magnetic particles, dispersed in a suitable liquid carrier (such as water, kerosene, diester, etc.), form a magnetic fluid. Their magnetic properties[12−17] cannot be analyzed without inclusion of the effects of size, shape, surface, polydispersity, and interactions between particles. For this reason, a method for synthesizing the particles with good control of these parameters is necessary. Hence several techniques have been used:

Ball milling[15,18] and a flame by vapor phase reaction and condensation[19] techniques have been employed to control the particle size (up to 10 nm) and morphology.

In aqueous solution, syntheses of magnetic spinel iron oxide have been performed through coprecipitation of various salts of Fe(III) and Fe(II) in alkaline media.[12,19−31] To obtain a spinel structure, the ratio Fe(II)/Fe(III) has

† URA CNRS 1662.
‡ CEA−CE Saclay.
* All correspondence to this author.
⊗ Abstract published in *Advance ACS Abstracts,* June 1, 1997.

(1) Special issue: Nanostructured Materials. *Chem. Mater.* **1996**, 8 (5).
(2) Pileni, M. P. *J. Phys. Chem.* **1993**, *97*, 6961.
(3) Pileni, M. P.; Motte, L.; Petit, C. *Chem. Mater.* **1992**, *4*, 338.
(4) Bawendi, M. G.; Steigerwald, M. L.; Brus, L. E. *Annu. Rev. Phys. Chem.* **1990**, *41*, 477.
(5) Petit, C.; Lixon, M. P.; Pileni, M. P. *J. Phys. Chem.* **1993**, *97*, 12974.
(6) Lisiecki, I.; Pileni, M. P. *J. Am. Chem. Soc.* **1993**, *115*, 3887.
(7) Gunther, L. *Phys. World* **1990**, *3*, 28.
(8) Ziolo, R. F. U.S Patent **1984**, *4*, 474.
(9) McMickael, R. D.; Shull, R. D.; Swartzendruber, L. J.; Bennett, L. H.; Watson, R. E. *J. Magn. Magn. Mater.* **1992**, *111*, 29.
(10) Anton, I.; De Sabata, I.; Vekas, L. *J. Magn. Magn. Mater.* **1990**, *85*, 219.
(11) Billas, M. L. I.; Châtelain, A.; de Heer, W. A. *Science* **1994**, *265*, 1682.
(12) Charles, S. W; Popplewell, J. *Ferromagnetic Materials*; Northholland Publishing Co.: Amsterdam, New York, Orford, 1982; Vol. 2.
(13) Haneda, K. *Can. J. Phys.* **1987**, *65*, 1233.
(14) Morrish, A. H. In *Studies of Magnetic Properties of Fine Particles and Their Relevance to Materials Science* Dormann, J. L., Fiorani, D., Eds.; Elsevier Science Publishers: Amsterdam, 1992; p 181.
(15) Berkowitz, A. E.; Lahut, J. A.; Jacobs, I. S.; Levinson, M.; Forester, D. W. *Phys. Rev. Lett.* **1975**, *34*, 594.
(16) Gangopadhyay, S.; Hadjipanayis, G. C.; Sorensen, C. M.; Klabunde, K. J. *IEEE Trans. Mag.* **1993**, *29*, 2619.
(17) Shinjo, T. *J. Phys. (Paris)* **1979**, *3*, 6.
(18) Papell, S. S. U.S. Patent 3,215,572, **1965**.
(19) Elmore, W. C. *Phys. Rev.* **1938**, *54*, 309.
(20) Jolivet, J. P.; Massart, R.; Fruchart, J. M. *Nouv. J. Chim.* **1983**, *7*, 325.
(21) Rosensweig, R. E.; Kaiser, R.; Miskolczy, G. *J. Colloid Interface Sci.* **1969**, *29*, 681.
(22) Tronc, E.; Belleville, P.; Jolivet, J. P.; Livage, J.; *Langmuir* **1992**, *8*, 313.
(23) Khalafalla, S. E.; Reimers, G. W. *IEEE Trans. Magn. Magn.* **1980**, *16*, 178.
(24) Sato, T.; Kuroda, C.; Saito, M.; Sugihara, M. In *Ferrites: Proceedings of the International Conference*; Hoshino, Y., Iida, S., Sugimoto, M., Eds.; University of Tokyo Press: Tokyo, Japan, 1971; p 72.
(25) Nakatsuka, K.; Jeyadevan, B. *IEEE Trans. Magn. Magn.* **1994**, *30*, 4671.
(26) Rozenberg, A. S.; Aleksandrova, E. I.; Dzhardimalieva, G. I.; Kir'yakov, N. V.; Chizhov, P. E.; Petinov, V. I.; Pomogailo, A. D. *Russ. Chem. Bull.* **1995**, *44*, 858.
(27) Vandenberghe, R. E.; Vandenberghe, R.; De Grave, E.; Robbrecht, G. *J. Magn. Magn. Mater.* **1980**, *15*, 1117.
(28) Sato, T.; Iijima, T.; Seki, M.; Inagaki, J. *J. Magn. Magn. Mater.* **1987**, *65*, 252.
(29) Davies, K. J.; Wells, S.; Charles, S. W. *J. Magn. Magn. Mater.* **1993**, *122*, 24.
(30) Davies, K. J.; Wells, S.; Upadhyay, R. V.; Charles, S. W.; O'Grady, K. O.; El Hilo, M.; Meaz, T.; Morup, S. *J. Magn. Magn. Mater.* **1995,** *149*, 14.
(31) Jolivet, J. P.; Belleville, P.; E. Tronc.; Livage, J. *Clays Clay Miner.* **1992**, *40*, 531.
(32) Taylor, R. M.; Schwertmann, U. *Clay Miner.* **1974**, *10*, 299.

S0743-7463(96)00854-2 CCC: $14.00 

to be higher than 0.4.[22] The syntheses are performed at very high salt and base concentrations.[12,22,23] The control of size, shape, and composition of $Fe_3O_4$ or $\gamma$-$Fe_2O_3$ nanoparticles[22,25−31] depends on the type of salt (chlorides, nitrates, perchlorates, etc.), the Fe(II) and Fe(III) ratio, and the pH and ionic strength of the media. The drastic changes in the experimental conditions to control the size induce a large modification in the particle interface (hydroxide formations, etc.). This modifies the magnetic properties[13−15] of the particles.

Syntheses performed with the presence of a high Fe(II) salt concentration and without Fe(III) derivatives[33−35] induce formation of $Fe_3O_4$ micrometer particles. The particle morphology depends critically on similar parameters described above (reactants concentrations, pH, ionic strength, etc.). According to the literature, it has been impossible to obtain particles in the nanosize range when Fe(II) salt is used for the synthesis. To obtain such particle size, the synthesis has to be performed with equal amounts of Fe(III) and Fe(II).

Organized assemblies have been used to control the particle size. Syntheses of $Fe_3O_4$ and $\gamma$-$Fe_2O_3$ nanosized particles have been performed in vesicles,[36] cast film,[37] bilayer lipid membrane,[38] polymer matrix,[39] and porous silica microspheres.[40] By using these organized assemblies, the particles formed are surrounded by surfactant molecules or polymers. As in syntheses carried out in homogeneous solutions, this induces marked changes at the surface of the particles and makes difficult deriving any relationship between magnetic properties and size.

In the last few years, we have developed a new technique for controlling the size of cobalt ferrite nanoparticles.[41−44] Oil in water functionalized micelles (the reactants are the counterions of the surfactants) are used. The surfactant is removed and the reactant concentration is very small. This allows to a first approximation, assuming that the particles from 2 to 5 nm keep the same surface area. For particles having average diameters of 2 and 3 nm, an axial anisotropy is observed whereas for larger sizes a cubic anistropy similar to the bulk phase is obtained.

Here, we demonstrate that this technique can be generalized to iron ferrite. The size of the particles varies from 3.7 to 11.6 nm. The size is controlled either by changing the micellar concentration by a factor of 4 or by increasing the temperature from 25 to 80 °C. The crystallinity of the particles depends markedly on the experimental mode. When the syntheses are performed at high temperatures (50 and 80 °C), the particles are well crystallized and the size varies from 6 to 11.6 nm. In contrast, at low temperatures, the crystallinity is very low. The magnetic properties depend on the particle size and, for a given size, on the crystallinity.

## II. Experimental Section

Sodium dodecyl sulfate, Na(DS), and ferrous chloride, $Fe(Cl)_2$, were from Fluka. All the compounds were stated to be 99.99% pure.

Transmission electron microscopy, TEM, and electron diffraction experiments were performed using a JEOL 100CX operating at 100 kV.

X-ray diffraction measurements were carried out by using a Stoe Stadi P goniometer and a Siemen Kristolloflex X-ray generator with a cobalt cathode driven by a personal computer through the Daco-PM interface.

The $^{57}$Fe Mössbauer absorption spectra at 77 K were recorded using a $^{57}Co^*$:Rh $\gamma$-ray source mounted on a triangular velocity electromagnetic drive.

The magnetic curves of ferrite powder, at room temperature, were determined by using a commercial alternative gradient magnetometer (Princeton Measurements Corp. Micomag, Model 2900) in a field up to 20 kOe.

When the particles were dispersed in a fluid, the magnetic curves were obtained by using a VSM magnetometer in a field up to 40 kOe. To prevent aggregation, magnetic particles were dispersed in 50% of ethylene glycol in water. Their weight fraction was kept constant at 0.4%.

## III. Size Determination by TEM

The mean diameter, $D_{TEM}$, and the standard deviation, $\sigma_{TEM}$, were derived from an average of 500 particles.

According to Chantrell et al.,[45] the best probability function is a log-normal distribution. From the best fit between the simulation and experimental data, the parameters $D_{TEM}$ and $\sigma_{TEM}$ were derived from the following equation

$$P(D) = \frac{1}{D_{TEM}\sigma_{TEM}(2\pi)^{1/2}}\exp\left(-\frac{\ln^2(D/D_{TEM})}{2\sigma_{TEM}^2}\right)$$

where $\sigma_{TEM}$ and ln $D_{TEM}$ are the standard deviation and the mean value of lnD, respectively. The maximum of $P(D)$ corresponds to a diameter, $D_{max}$:

$$D_{max} = D_{TEM}\exp(-\sigma_{TEM}^2)$$

## IV. Treatment of Magnetic Data

Single-domain nanoparticles characterized by a diameter, $D_{MD}$, have superparamagnetic behavior and are described by the Langevin function[46]

$$M = M_s(\coth(x) - 1/x)$$

where

$$x = \frac{\mu(D_{MD})H}{kT}$$

with

$$\mu(D_{MD}) = \frac{m_s D_{MD}^3 \pi}{6}$$

$M_s$ and $m_s$ are the saturation magnetization of nanoparticles and the bulk phase, respectively.

For a very small magnetic field, $\chi$ is negligible compared to one and the magnetization can be expressed

(33) Matijevic, E. *Chem. Mater.* **1993**, *5*, 412.
(34) Sugimoto, T.; Matijevic, E. *J. Colloid Interface Sci.* **1980**, *74*, 227.
(35) Domingo, C.; Rodriguez-Clemente, R. *Mater. Res. Bull.* **1991**, *26*, 47.
(36) Mann, S.; Sparks, H. C.; Board, R. G. *Adv. Microb. Physiol.* **1990**, *31*, 125.
(37) Okada, K.; Sakata, K.; Kunitake, T. *Chem. Mater.* **1990**, *2*, 89.
(38) Zhao, X. K.; Herve, P. J.; Fendler, J. H. *J. Phys. Chem.* **1989**, *93*, 908.
(39) Ziolo, R. F.; Giannelis, E. P.; Weinstein, B. A.; O'Horo, M. P.; Ganguly, B. N.; Mehrotra, V.; Russell, M. W.; Huffman, D. R. *Science* **1992**, *257*, 219.
(40) Zhang, M.; Zhang, Q., Itoh, T.; Abe, M. *IEEE Trans. Magn. Mag.* **1994**, *30*, 4692.
(41) Moumen, N.; Veillet, P.; Pileni, M. P. *J. Magn. Magn. Mater.* **1995**, *149*, 67.
(42) Moumen, N.; Pileni M. P. *J. Phys. Chem.* **1996**, *100*, 1867.
(43) Moumen, N.; Pileni M. P. *Chem. Mater.* **1996**, *8*, 1128.
(44) Moumen, N.; Lisiecki, I.; Briois, V.; Pileni, M. P. *Supramol. Sci.*, in press.
(45) Chantrell, R. W.; Popplewell, J.; Charles, S. W. *Physica* **1977**, *86-88B*, 1421.
(46) Neel, L. *Ann. Geophys.* **1949**, *5*, 99.

$$M \simeq \frac{x}{3} = \frac{M_s \mu \mathrm{H}}{3kT}$$

Thus, it is possible to give a simpler expression for initial susceptibility:

$$\chi_i = \frac{M_s \mu}{3kT}$$

This is valid for a monodispersed distribution. The size polydispersity has to be introduced through a log-normal distribution:

$$M = \int_0^{+\infty} M(D_{\mathrm{MD}}) P(D_{\mathrm{MD}})\, \mathrm{d}D_{\mathrm{MD}}$$

and

$$\bar{\chi}_i = \frac{\chi_i}{M_s} = \frac{m_s \pi}{18kT} \int_0^{+\infty} {D_{\mathrm{MD}}}^3 P(D_{\mathrm{MD}})\, \mathrm{d}D_{\mathrm{MD}}$$

The superparamagnetic nanoparticles are ferri- or ferromagnetic single-domain particles so small that the thermal energy is the order of magnitude of the anisotropy energy barrier. Without an applied magnetic field, for an assembly of particles, magnetic moment directions are redistributed by thermal fluctuations and the particles exhibit no remanence.

## V. Synthesis of Ferrous Dodecyl Sulfate

Ferrous dodecyl sulfate is made by mixing an aqueous solution of sodium dodecyl sulfate with ferrous chloride, as described elsewhere.[47] An aqueous solution of 0.1 M of sodium docedyl sulfate is mixed with 0.1 M of ferrous chloride. The solution is kept at 2 °C and a precipitate appears. It is washed several times with a 0.1 M ferrous chloride solution and recrystallization in distilled water. Ferrous dodecyl sulfate, $Fe(DS)_2$, forms micellar aggregates above the critical micellar concentration, cmc of $1.4 \times 10^{-3}$ M. The shape and the size of these aggregates have been determined by small angle X ray scattering and by light scattering.[48] They were found to be prolate ellipsoidal micelles with a hydrodynamic radius of 2.7 nm.

## VI. Results and Discussion

**VI-1. Synthesis and Characterization of Ferrite Nanosized Particles.** Ferrous dodecyl sulfate, $[Fe(DS)_2] = 10^{-2}$ M, is solubilized in aqueous solution and methylamine, $[CH_3NH_3OH] = 0.77$ M, added to the micellar solution. After the solution is stirred for 3 h at 50 °C with air presence, a magnetic precipitate appears. The supernatant is removed and replaced by aqueous solution, and after several washings, the precipitate is redispersed in aqueous solution thus obtaining a magnetic fluid. The percentage of surfactant remaining in solution is less than 0.1 wt %. To obtain a dry powder, the solvent is removed by freeze drying. From the electron micrograph pattern (Figure 1A), the average diameter is 7.4 nm. From electron and X-ray diffraction, the peaks listed in standard reference tables clearly indicate formation of an inverted spinel crystalline structure. To differentiate between $Fe_3O_4$ and $\gamma$-$Fe_2O_3$ nanoparticles, the main peak is enhanced. Figure 2 shows the X-ray diffraction patterns obtained immediately after synthesis and 1 month later

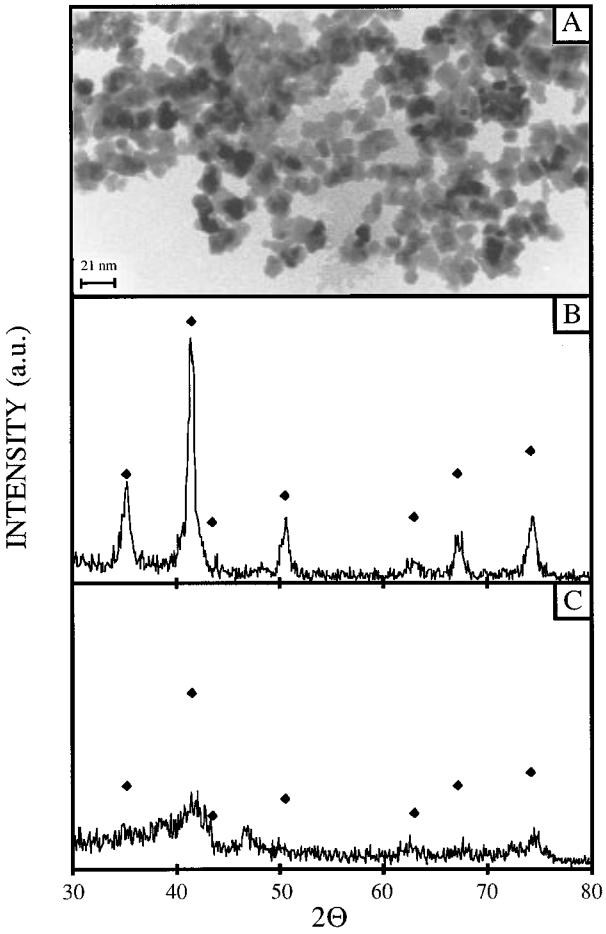


**Figure 1.** (A) Electron microscopy pattern of magnetic fluid made with $[Fe(DS)_2] = 10^{-2}$ M at $T = 50$ °C, keeping $[CH_3NH_3OH]/[Fe(DS)_2] = 77$. (B) X-ray diffraction pattern of $Fe_3O_4$ nanoparticles made from micelles $[Fe(DS)_2] = 10^{-2}$ M at $T = 50$ °C. The average size determined by TEM is 7.4 nm. (C) X-ray diffraction pattern of $Fe_3O_4$ nanoparticles made from micelles, $[Fe(DS)_2] = 10^{-2}$ M at $T = 25$ °C. The average size determined by TEM is 7 nm .

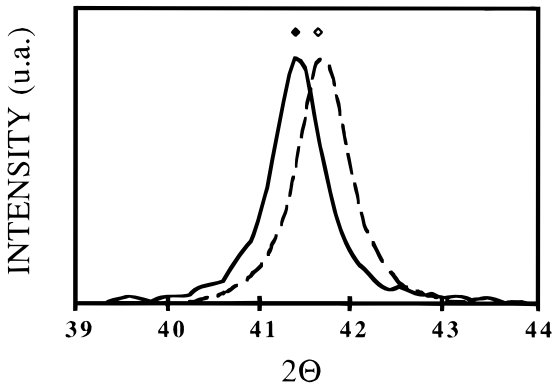


**Figure 2.** X-ray diffraction pattern of nanoparticles made from micelles $[Fe(DS)_2] = 10^{-2}$ M at $T = 50$ °C and with an average diameter of 7.4, immediately (—) and 1 month (- - -) after the synthesis.

(the powder was kept under normal laboratory conditions). Immediately after synthesis, the mean peak is centered at 41.39° whereas in the older sample it is at 41.62°. This shift in the maximum is attributed to the oxidation of the $Fe_3O_4$ to $\gamma$-$Fe_2O_3$ nanoparticles. A Mössbauer spectrum (Figure 3), obtained with the same older sample at 77 K, exhibited the hyperfine splitting pattern (sextet) characterizing $\gamma$-$Fe_2O_3$ with a hyperfine field of 513 kOe. The shape of the Mössbauer spectrum and the hyperfine field

(47) Moroi, Y.; Motomura, K.; Matuura, R. *J. Colloid Interface Sci.* **1974**, *46*, 111.

(48) Petit, C.; Jain, T. K.; Billoudet, F.; Pileni, M. P. *Langmuir* **1994**, *10*, 4446.

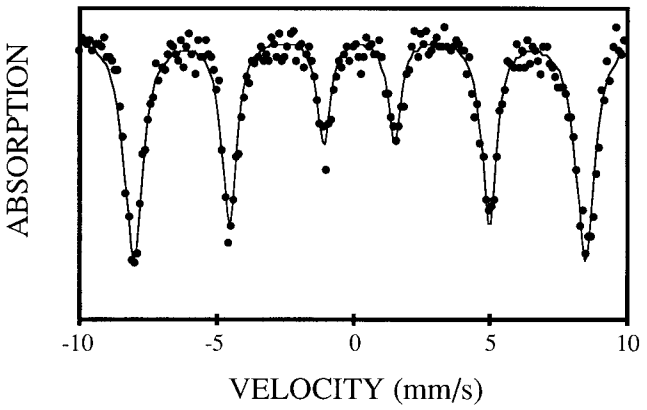


**Figure 3.** Mössbauer spectrum at 77 K of 7.4 nm diameter particles, ($[Fe(DS)_2] = 10^{-2}$ M at $T = 50$ °C).

value are in good agreement with the published data previously.[49,50] Fe(II) cannot be detected in the Mössbauer spectrum indicating that only trace amounts of $Fe_3O_4$ could be present.

The formation mechanism of stoichiometric $Fe_3O_4$ nanoparticles is probably similar to that obtained in aqueous solution, as described previously.[22,31] Iron(II) and -(III) react with hydroxide groups produced by methylamine dissociated in aqueous solution. In its crystalline form $Fe(OH)_2$, reacts with $Fe(OH)_3$ to form $Fe_3O_4$. Formation of $\gamma$-FeOOH as intermediate cannot be excluded.[51] However, there are the following drastic differences in the experimental conditions:

(i) Formation of $Fe_3O_4$ is observed at low reactant concentration ($2.5 \times 10^{-3}$ M < $[Fe(DS)_2]$ < $10^{-2}$ M) whereas it is impossible in homogeneous solution. This is attributed to formation of micelles with a high local concentration of Fe(II) in the Stern layer. This is confirmed by the fact that below the cmc ($1.3 \times 10^{-3}$ M) $Fe_3O_4$ is not formed.

(ii) In homogeneous solution, the syntheses are performed at high temperature. Futhermore, in the absence of Fe(III) salt formation of large (micrometer) and well-defined particles is observed.[33−35] In micellar solution, nanosized particles are obtained at room temperature. These differences can be attributed to the fact the oxygen solubility is higher in micellar than in aqueous solutions. This favors the formation of $Fe(OH)_3$ and then $Fe_3O_4$.[31] This process occurred in a supersaturated medium and can be related to formation of magnetite in biomineralization organisms. In these organisms formation of biological $Fe_3O_4$ occurs at room temperature whereas in homogeneous solution the ferrite plating is obtained above 60°C.[51]

The size is controlled by changing either temperature or $Fe(DS)_2$ concentration with $[CH_3NH_3OH]/[Fe(DS)_2] = 77$. Figures 4 and 5 show the electron micrograph patterns and histograms obtained at various $Fe(DS)_2$ concentrations and temperatures. With an increase of either the $Fe(DS)_2$ concentration or temperature, an increase in the particle size is observed. Nanoparticles synthesized at a temperature higher than or equal to 50 °C are characterized by a well-defined X-ray diffraction pattern. This indicates formation of highly crystallized nanoparticles. Conversely, when the syntheses are performed at 25 °C, the X-ray diffraction pattern indicates formation of particles with a low crystallinity. Parts B and C of Figure 1 compare X-ray patterns of similar sized (7.4 nm and 7 nm) nanoparticles from the syntheses at 25 and 50 °C. A peak at 47° can be observed in X-ray diffraction patterns obtained at 25 °C. No peaks in the standard tables corresponding to oxide derivatives are found. This peak could be attributed to remaining surfactant with a low crystallinity.

At a fixed temperature, the increase in the particle size with increasing $Fe(DS)_2$ concentration cannot be explained in terms of changes of the structural micellar structure. Preliminary results obtained by small angle X-ray spectroscopy (SAXS) indicate no change in the size and the shape of the micelles.[52] The size control with the surfactant concentration is attributed to the increase in oxygen solubility with the increase of micellar concentration. This favors an increase in the oxidation from $Fe^{2+}$ to $Fe^{3+}$ and then induces, as in homogeneous solution,[31] an increase in the particle size.

At fixed $Fe(DS)_2$ concentration, the increase in the particle size with temperature can be related to an increase in the degree of micellar ionization[53] and to oxygen solubility. Again, these two parameters favor formation of $Fe^{3+}$ ions and then induce an increase in the particle size.

**VI-2. Magnetic Properties. VI-2-1. In Powder Form**. The magnetization curves of different sized nanoparticles were obtained at 300 K. The magnetic properties depend on particle size and synthesis mode:

(i) The smallest particle size is obtained when the particles are synthesized at 25 °C (Figures 4 and 5). Parts A−C of Figure 6 show the magnetization curves of particles having average diameters of 3.7, 5.6, and 7 nm, respectively. No reduced remanence and coercivity are observed. Hence, to a first approximation, superparamagnetic behavior is assumed. The saturation magnetization, $M_s$, is not reached even for a 20 kOe magnetic field and is derived from extrapolation of $M$ vs $1/H$ to zero (Table 1). The magnetic size is derived from the Langevin equation assuming a log normal size distribution.[45] Good agreement between the simulated and experimental magnetization curve is obtained (Figure 6A−C). However, the magnetic diameters are smaller than those determined by TEM (Table 1).

(ii) When the syntheses are performed at 50 and 80 °C, as above, the size of the particles increases with increasing $Fe(DS)_2$ concentration. The magnetization curves show reduced remanence and coercivity with the increase in the particle size. The saturation magnetization, $M_s$, is reached when the applied field is 15 kOe. Parts A−C of Figure 7 show such behavior for particles made at 80 °C and characterized by average diameters of 6.6, 8.3, and 11.6 nm, respectively. Table 1 shows that the coercivities remain rather low. When the particles are superparamagnetic, the magnetic diameters determined from simulation of the magnetization curves are higher than those determined by TEM (Table 1).

From what is described above, the synthesis temperature plays an important role. This is summarized as follows:

(i) The saturation magnetization, $M_s$, is not reached at 20 kOe for particles made at 25 °C whereas it is observed at 15 kOe for higher temperatures (Figures 6 and 7).

(ii) The magnetic diameters are smaller at 25 °C and larger at higher temperatures compared to those determined by TEM (Table 1).

(iii) The X-ray diffraction patterns show very low crystallinity for particles made at 25 °C compared to those made at and above 50 °C (Figure 1B,C).

(49) Koutani, S.; Gavalle, G.; Gerardin, R. *J. Magn. Magn. Mater.* **1993**, *123*, 175.
(50) Batis-Landoulsi, H.; Vergnon, P. *J. Mater. Sci.* **1983**, *18*, 3399.
(51) Abe, M.; Itoh, T.; Tamaura, Y. *Thin Solid Films* **1992**, *216*, 155.
(52) Lisiecki, I.; Dias, O.; Pileni, M. P. Unpublished data.

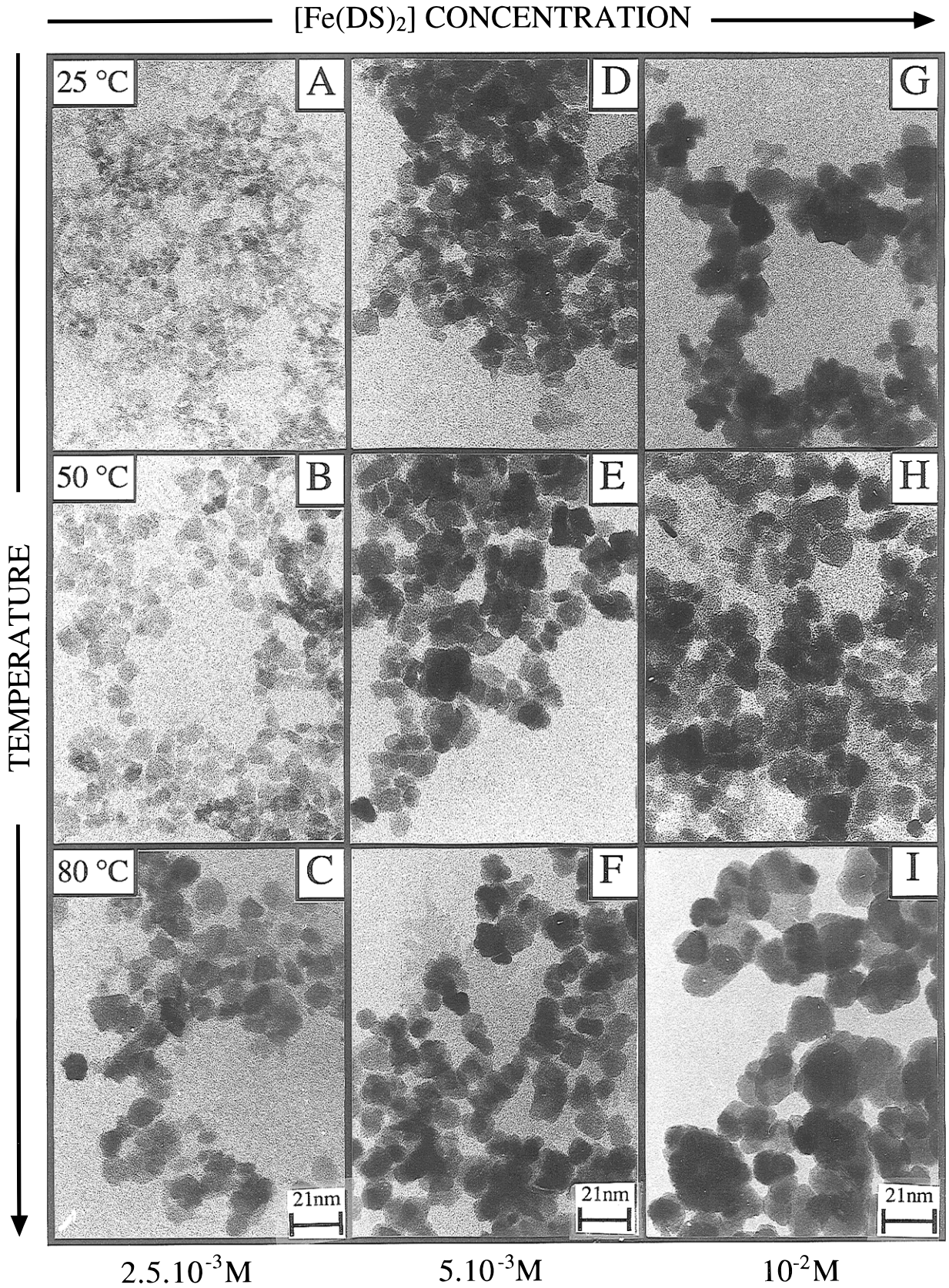


**Figure 4.** Electron microscopy patterns of magnetic fluids made at various surfatant concentrations and temperatures, keeping $[CH_3NH_3OH]/[Fe(DS)_2] = 77$: $[Fe(DS)_2] = 2.5 \times 10^{-3}$ M, $T = 25$ °C (A); $[Fe(DS)_2] = 2.5 \times 10^{-3}$ M, $T = 50$ °C (B); $[Fe(DS)_2] = 2.5 \times 10^{-3}$ M, $T = 80$ °C (C); $[Fe(DS)_2] = 5 \times 10^{-3}$ M, $T = 25$ °C (D); $[Fe(DS)_2] = 5 \times 10^{-3}$ M, $T = 50$ °C (E); $[Fe(DS)_2] = 5 \times 10^{-3}$ M, $T = 80$ °C (F); $[Fe(DS)_2] = 10^{-2}$ M, $T = 25$ °C (G); $[Fe(DS)_2] = 10^{-2}$ M, $T = 50$ °C (H); $[Fe(DS)_2] = 10^{-2}$ M, $T = 80$ °C (I).

These data suggest, for particles synthetized at 25 °C, low crystallinity at the interface. This induces a change in the magnetocrystalline anisotropy. The difference between the magnetic and TEM diameters is explained as follows: When the particles are characterized by high crystallinity, the interactions between particles are rather large whereas the opposite is true for particles with low crystallinity. The magnetic size of $CoFe_2O_4$ nanoparticles dispersed in a fluid (with 0.1% volume fraction) and in powder form are compared in previous papers.[43] In fluids,

**Table 1. Properties of Particles Prepared Using Various $Fe(DS)_2$ Concentrations and Temperatures[a]**

| | $2.5 \times 10^{-3}$ M 25 °C | $2.5 \times 10^{-3}$ M 50 °C | $2.5 \times 10^{-3}$ M 80 °C | $5 \times 10^{-3}$ M 25 °C | $5 \times 10^{-3}$ M 50 °C | $5 \times 10^{-3}$ M 80 °C | $10 \times 10^{-3}$ M 25 °C | $10 \times 10^{-3}$ M 50 °C | $10 \times 10^{-3}$ M 80 °C |
|---|---|---|---|---|---|---|---|---|---|
| $D_{TEM}$ (nm) | 3.7 | 6 | 6.6 | 5.6 | 6.8 | 8.3 | 7 | 7.4 | 11.6 |
| $\sigma_{TEM}$ (%) | 33 | 34 | 25 | 34 | 26 | 28 | 33 | 24 | 22 |
| $D_{MD}$ (nm) | 2.4 | | 8.5 | 3.6 | 10.2 | 10.2 | 5.6 | 10.5 | |
| $\sigma_{MD}$ (%) | 40 | | 43 | 39 | 40 | 40 | 55 | 30 | |
| $H_{CD}$ (Oe) | | | | | | 33 | | 24 | 78 |
| $M_{SD}$ (emu/g) | 5 | | 30 | 6 | 33 | 33 | 11 | 46 | 55 |
| $\chi_{MD}$ (emu/g Oe) $\times 10^4$ | 0.4 | | 500 | 8 | 740 | 500 | 80 | 880 | 700 |
| $M_{SF}$ (emu/g) | 7.6 | 9.3 | 31 | 18.3 | 43 | 45 | 18.2 | 31 | 35.3 |
| $H_{CF}$ (Oe) | | | | | | 110 | | 250 | 215 |

[a] $D_{TEM}$ (nm), average diameter of the particles derived from TEM; $\sigma_{TEM}$, size polydispersity determined by TEM; $D_{MD}$ (nm), $\sigma_{MD}$, average diameter and size polydispersity of dry powder particles derived from simulation; $\chi_{MD}$, susceptibility in dry particles at room temperature; $H_{CD}$ (Oe) and $H_{CF}$ (Oe), coercivity in dry powder and in fluid; $M_{SD}$ and $M_{SF}$, saturation magnetization in dry powder and in magnetic fluid.

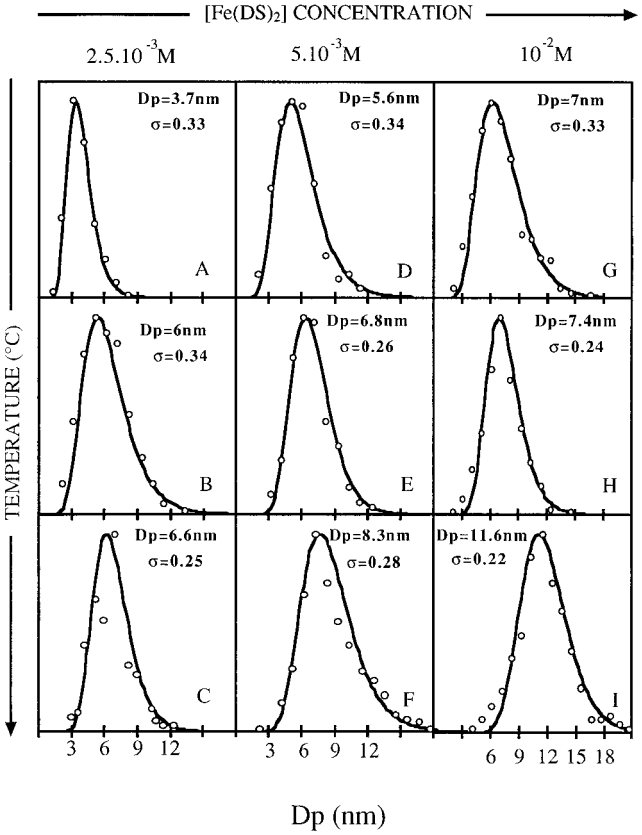


**Figure 5.** Histograms of magnetic fluids made at various surfatant concentrations and temperatures, keeping $[CH_3NH_3OH]/[Fe(DS)_2] = 77$: $[Fe(DS)_2] = 2.5 \times 10^{-3}$ M, $T = 25$ °C (A); $[Fe(DS)_2] = 2.5 \times 10^{-3}$ M, $T = 50$ °C (B); $[Fe(DS)_2] = 2.5 \times 10^{-3}$ M, $T = 80$ °C (C); $[Fe(DS)_2] = 5 \times 10^{-3}$ M, $T = 25$ °C (D); $[Fe(DS)_2] = 5 \times 10^{-3}$ M, $T = 50$ °C (E); $[Fe(DS)_2] = 5 \times 10^{-3}$ M, $T = 80$ °C (F); $[Fe(DS)_2] = 10^{-2}$ M, $T = 25$ °C (G); $[Fe(DS)_2] = 10^{-2}$ M, $T = 50$ °C (H); $[Fe(DS)_2] = 10^{-2}$ M, $T = 80$ °C (I).

the magnetic diameters are in good agreement with those determined by TEM whereas they are larger in powder form.

For any preparation mode, the saturation magnetization increases with the increase in the particle size but never reaches that obtained in the bulk phase (73.6 emu·g$^{-1}$).[54] Figure 8 shows the decrease in the saturation magnetization with the increase in the specific surface. Mollard et al.[55] found a linear relationship between the saturation magnetization and the specific surface. From extrapolation to zero magnetization, they deduced formation of a

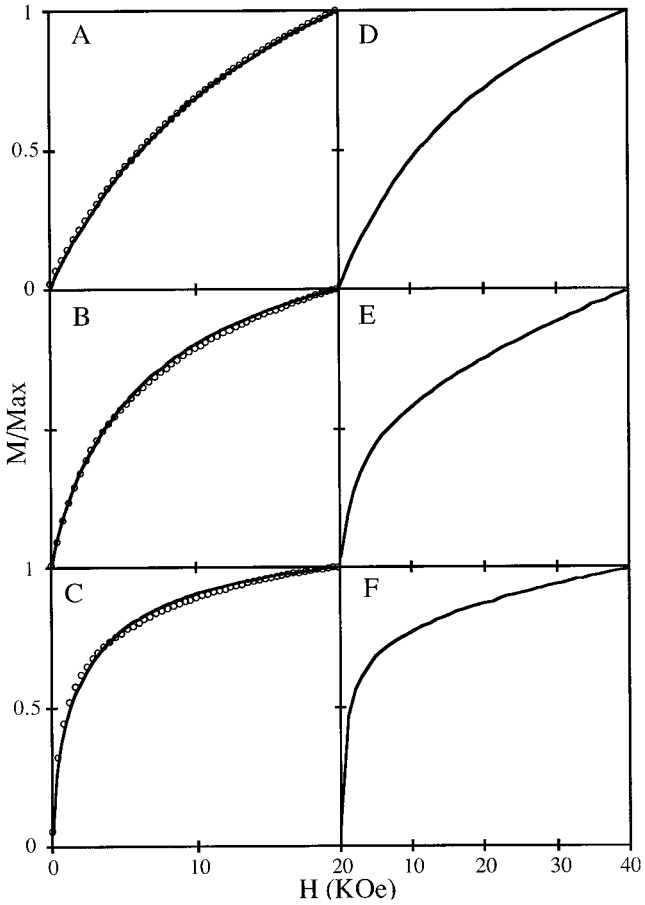


**Figure 6.** Variation of the magnetization with the increase in particle size obtained from powder at 300 K (A), (B), and (C) and from fluid at 200 K (D), (E), and (F), respectively. The magnetic particle diameter, $D_{MD}$, and the standard distribution, $\sigma_{MD}$, are 2.4 nm ($\sigma_{MD} = 0.4$) (A and D), 3.6 nm ($\sigma_{MD} = 0.39$) (B and E), and 5.6 nm ($\sigma_{MD} = 0.55$) (C and F), respectively. The experimental conditions are as follows: $[Fe(DS)_2] = 2.5 \times 10^{-3}$ M, $T = 25$ °C (A) and (D); $[Fe(DS)_2] = 5 \times 10^{-3}$ M, $T = 25$ °C (B) and (E); $[Fe(DS)_2] = 10^{-2}$ M, $T = 25$ °C (C) and (F).

"dead layer" surrounding the particles. From Figure 8, no linear relationship is observed and the saturation magnetization never reaches zero. This indicates that the assumption of "dead layer" formation can be excluded. These results are explained in terms of an increase in the noncollinearity of the magnetic structure.

The reduced magnetic susceptibility is obtained by dividing the value of the initial slope of the magnetization by the saturation magnetization. The reduced susceptibility can be calculated from the diameter and its standard deviation. Figure 9 shows rather good agree-

(53) Hayter, J. B. *Langmuir* **1992**, *8*, 2873.
(54) Bacri, J.-C.; Perzynski, R.; Salin D.; Cabuil V.; Massart R. *J. Magn. Magn. Mater.* **1986**, *62*, 36.
(55) Mollard, P.; Germi, P.; Rousset, A. *Physica B+C* **1977**, *86–88*, 1393.

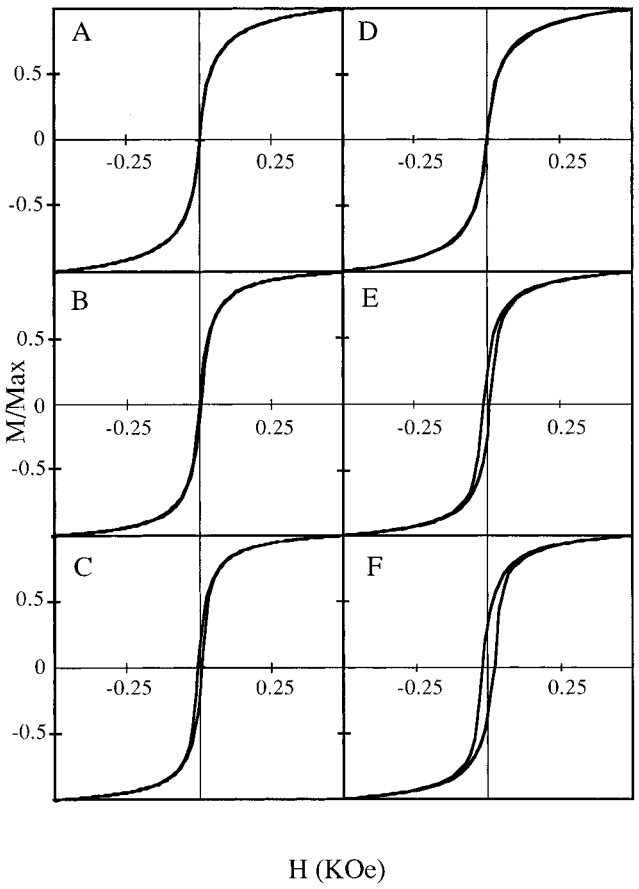


**Figure 7.** Variation of the magnetization with the increase in particle size obtained from powder at 300 K (A), (B), and (C) and from fluid at 200 K (D), (E), and (F), respectively. The TEM diameters and the standard distribution, $\sigma_{TEM}$, are 6.6 nm ($\sigma_{TEM}$ = 0.25) (A and D), 8.3 nm ($\sigma_{TEM}$ = 0.28) (B and E), and 11.6 nm ($\sigma_{TEM}$ = 0.22) (C and F), respectively. The experimental conditions are as follows: $[Fe(DS)_2] = 2.5 \times 10^{-3}$ M, $T$ = 80 °C (A) and (D); $[Fe(DS)_2] = 5 \times 10^{-3}$ M, $T$ = 80 °C (B) and (E); $[Fe(DS)_2] = 10^{-2}$ M, $T$ = 80 °C (C) and (F).

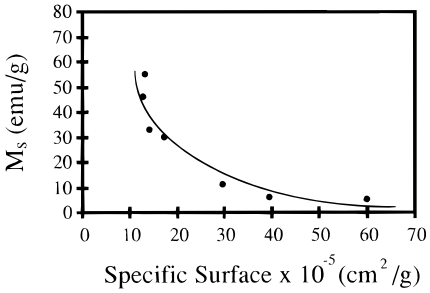


**Figure 8.** Variation of the saturation magnetization with the specific surface.

ment between the calculated and experimental data which confirms the superparamagnetic behavior of the nanoparticles.

**VI-2-2. Comparison of the Magnetic Behavior of Particles Dispersed in Fluid and in Powder Form.** With the particles dispersed in a fluid (particle volume fraction 0.4%), the magnetic properties were studied, at 200 and 300 K and with powder, and the magnetization was measured at 300 K. Comparison of the behavior of magnetic properties in powder form and fluid gives rather surprising results and shows that these differ markedly with the particle size:

(i) For the smallest size, superparamagnetic behavior is observed, in powder (Figure 6A−C) and in fluid (Figure 6D−F). This is very well confirmed by the superposition

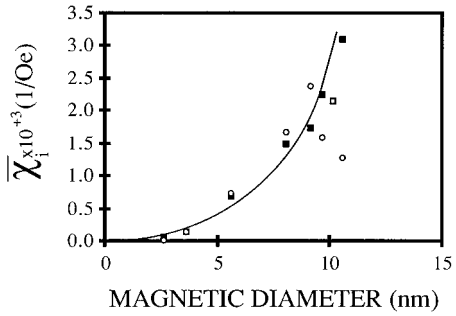


**Figure 9.** Variation of the reduced susceptibility with the magnetic diameter.

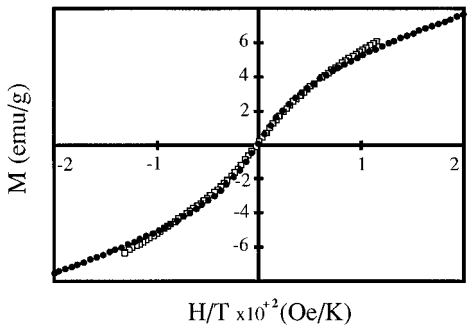


**Figure 10.** Magnetization curves of magnetic fluid formed with particles having an average magnetic diameter of 2.6 nm at room temperature (□) and 200 K (●).

of the magnetic curves of particles dispersed in a fluid recorded at 200 and 300 K, respectively (Figure 10).

(ii) For larger particles dispersed in a fluid, the progressive appearance of the remanence and the coercivity when the size increases from 8.3 to 11.6 nm is shown in Figure 7D−F (Table 1). This is more pronounced in fluid than in powder. This can be attributed to the fact that the blocking temperature of $\gamma$-$Fe_2O_3$ particles having an average diameter up to 7 nm is 200 K. These data confirm Koutani et al's[49] results for particles having an average diameter of 8 nm.

## VIII. Conclusion

In this paper, we demonstrate the formation of different-sized iron ferrite nanoparticles. To obtain such particles, oil in water micelles have to be formed. The syntheses are possible at room temperature and at very low Fe(II) concentration and under these conditions, nanoparticles are obtained whereas in homogeneous solution syntheses using Fe(II) induce formation of particles in the micrometric range. The particle size is controlled either at a fixed temperature by increasing $Fe(DS)_2$ concentrations or at a fixed $Fe(DS)_2$ concentration and various temperatures. When the particles are synthesized at 25 °C, their crystallinity is rather low and they behave as smaller magnetic particles. At 50 °C and above, the crystallinity is high and the magnetic properties change with the particle size which varies from 3.7 to 11.6 nm diameter. Large changes in the magnetization behavior are observed when the particles are dispersed in a fluid or in powder. The blocking temperature of the particles having a diameter larger than 7 nm is found to be close to 200 K.

**Acknowledgment.** The authors thank Dr. P. Veillet for use of the AGFM equipments and Dr. J. P. Bonville for providing the Mössbauer spectrum. The VSM experiments were performed at the Institut Louis Néel in Grenoble, and we are most grateful to Dr. B. Barbara, L. Thomas, and F. Lionty for their hospitality.

LA960854Q